JCTC Journal of Chemical Theory and Computation

Article

pubs.acs.org/JCTC

Toward a Broadly Applicable Force Field for d^6-Piano Stool Complexes

Maurus H. Schmid,[†,‡] Thomas R. Ward,*[,†] and Markus Meuwly*[,‡]

[†]Department of Chemistry, University of Basel, Spitalstrasse 51, CH-4056 Basel, Switzerland

[‡]Department of Chemistry, University of Basel, Klingelbergstrasse 80, CH-4056 Basel, Switzerland

Supporting Information

ABSTRACT: Three-legged piano stool complexes are prototypical organometallic complexes relevant to a wide range of chemically relevant questions. Force field parametrization of transition-metal complexes is difficult and underdeveloped, and metal-specific force fields and software are required. Here we report our efforts to derive parameters for the conventional CHARMM and the Valbond-CHARMM force fields for d^6-piano stool complexes. In Valbond-CHARMM, the usual angular term is replaced with hybrid orbital strength functions. These functions describe the energy not only of distorted bond angles around the minimum but also at very large distortions. Structure optimizations led to a good agreement between the calculated force field and the X-ray structures. They were comparable to RMSDs obtained between X-ray and DFT structures. In addition, and contrary to treating the systems with DFT, molecular dynamics simulations on the multiple nanosecond time scale are possible and allow to compute meaningful structural and energetic observables. Explicit solvent simulations of the complexes in methanol and water allow to determine the solvent distribution around the complexes. The parametrization presented here will be a useful starting point for dynamics investigations of catalysts in structurally more demanding environments.

INTRODUCTION

Three-legged piano stool complexes are prototypical organometallic complexes. Over the years they have received increasing attention as catalyst precursors as well as organometallic building blocks which can act either as enzyme inhibitors or metalloenzyme mimetics.[1−4] To complement experiments, interpret observations, or even predict experimental findings, computational modeling is a valuable and often indispensable tool. Computational investigations of these complexes have traditionally used ab initio methods or density functional theory (DFT). However, with in silico high-throughput screening approaches in mind, the computational power required even with DFT becomes prohibitive. For studies of organometallic complexes together with metalloenzymes, mixed quantum mechanical/molecular mechanics (QM/MM) procedures may be attractive, but for library-screening purposes such an approach is not sufficiently efficient and scalable. Instead, force field methods would be highly desirable. As force field calculations are much faster than any of the QM methods, they not only allow screening of large libraries but also explicit atomistic simulations of much larger systems involving proteins including artificial metalloenzymes or enzymes with transition-metal inhibitors mentioned above.

Most general purpose force fields for atomistic simulations (e.g., CHARMM,[5] Amber,[6] Gromos[7] or OPLS[8]) are defined as a sum of bonded and nonbonded energies:

$$V = E_{\text{bonded}} + E_{\text{nonbonded}} \tag{1}$$

The bonded energies are sums over harmonic potentials for stretching and bending terms and periodic functions for torsions:

$$E_{\text{bonded}} = \sum_{\text{bonds}} k_r(r - r_0)^2 + \sum_{\text{angles}} k_\theta(\theta - \theta_0)^2 + \sum_{\text{torsion}} k_\gamma(1 + \cos(n\omega - \gamma)) + \sum_{\text{improper}} k_\phi(\phi - \phi_0)^2 \tag{2}$$

Additional terms such as Urey−Bradley terms are commonly included as well. The nonbonded terms include sums over electrostatic (point charge) and vdW terms.

$$E_{\text{nonbonded}} = \sum_{i<j} \left\{ 4\varepsilon_{ij} \left[\left(\frac{\sigma_{ij}}{r_{ij}} \right)^{12} - \left(\frac{\sigma_{ij}}{r_{ij}} \right)^{6} \right] + \frac{q_i q_j e^2}{r_{ij}} \right\} \tag{3}$$

Metallocene and bent-metallocene complexes have been parametrized in a few instances.[9−11] But generally, force field parametrization of transition-metal complexes is difficult and underdeveloped, and metal-specific force fields and software are required,[12−19] as it has been suggested that the harmonic

Received: December 10, 2012
Published: March 13, 2013

approximation for bonds and angles may not be the most suitable for transition metals.[17,18,20,21]

In order to describe ground-state geometries, a considerable number of force field parameters is required: every bond length, angle, and dihedral angle requires at least two parameters. In this context, the Valbond (VB)[22] formalism alleviates some of these drawbacks for the angular terms. Instead of two parameters (force constant and equilibrium angle) for each atom type triad, VB requires a hybridization for each atom, which is usually determined automatically but can be assigned by the user, and only one parameter per element pair to describe the bond hybridization. This reduces the parametrization effort, especially for complicated structures with many different atom types. For example, for the most simple complex **1** (see Figure 1), 6 VB instead of 20 CHARMM angle parameters are needed. For the more complex case of compound **4**, VB requires 7 parameters, whereas CHARMM requires more than 60.

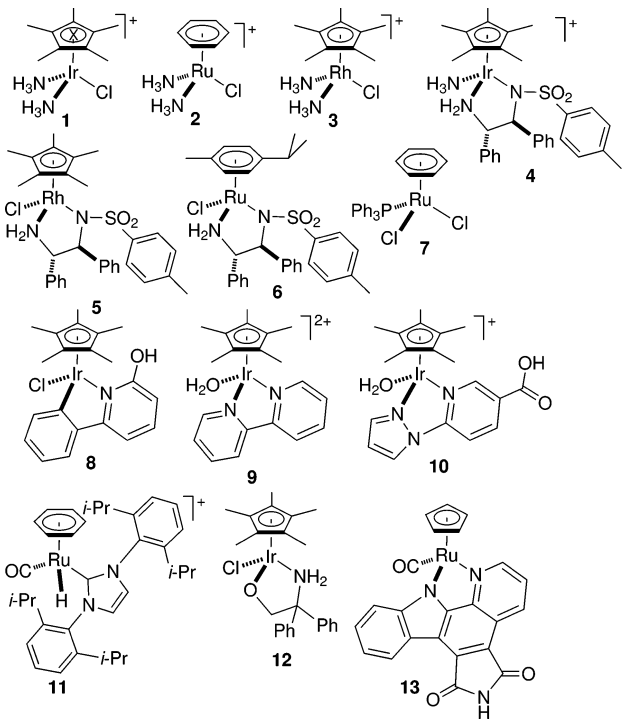

Figure 1. Representative three-legged piano stool complexes used in this study. Model compounds **1**–**3** are DFT structures, and the remaining complexes **4**–**13** are X-ray structures extracted from the CSD (**4**–**12**) or PDB (**13**).

VB[22−24] is based on valence bond theory as originally developed by Pauling.[25] It replaces the conventional harmonic bending term in a general-purpose force field with the VB-energy expression which is based on hybrid orbital strength functions as the basis for a molecular mechanics expression. These functions not only describe the energy of bond angles around the minimum but also at larger distortions where the harmonic approximation breaks down. In this fashion, VB can reproduce unusual geometries as illustrated by the distorted trigonal prism reported for $[W(CH_3)_6]$.[26] More recently, we extended the VB formalism to include the *trans*-influence which yields VB-trans (VBT).[19]

For an angle α between nonhypervalent bonds with an $sp^m d^n$ hybrid orbital, the overlap between the orbitals, Δ, is expressed as a function of the hybridizations m and n and the angle:

$$\Delta = \frac{1}{1+m+n}\left(1 + m\cos\alpha + \frac{n}{2}(3\cos^2\alpha - 1)\right) \quad (4)$$

The overlap is used to define the strength function S:

$$S(\alpha) = S^{\max}\sqrt{1 - \frac{1-\sqrt{1-\Delta^2}}{2}} \quad (5)$$

where $S^{\max}$ is the maximum overlap between the orbitals:

$$S^{\max} = \sqrt{\frac{1}{1+m+n}}\,(1 + \sqrt{3m} + \sqrt{5n}) \quad (6)$$

The energy contribution of one (bond-)orbital to the angular energy is

$$E_{\text{angle}} = k(S^{\max} - S(\alpha)) \quad (7)$$

The parameter k is a scaling constant for the interactions between the atom at the center of the angle with one of its bonding partners. VB also supports hypervalent compounds using a three-center four-electron bonding model.[23,24] For transition metals, VB traditionally considers only sd hybrids. Thus complexes that count more than 12 electrons in their valence orbitals are considered hypervalent and three-center four-electron bonds are used instead of the p-orbitals.

An additional advantage of VB over conventional force fields is that it requires considerably fewer angle parameters; only one parameter is required for every pair of bonded atoms. The remaining parameters (bonds, dihedral, nonbonding, etc.) are identical to those used in the standard CHARMM force field. However, partial optimizations of these parameters are likely to be necessary for a robust force field including specific metals in their different oxidation states. In addition, assignment of a hybridization is not always trivial and needs careful exploration for more complicated cases, such as the piano stool complexes in the present study. The determination and validation of such a parametrization is the main subject of the present contribution. In our implementation of VB and VBT[19] (available from CHARMM[5] version 37 onward), the conventional CHARMM angle terms are replaced by more realistic combinations of hybrid orbitals which can be assigned by the user. In this way, VB and VBT can be combined and are compatible with the conventional CHARMM force field and simulations in a variety of ways are possible, as will be explained further below. Recently, MacKerell et al. have introduced the CHARMM general force field (CGenFF[27] which also provides a convenient fitting environment (https://www.paramchem.org) for automatically generated parameters.[28,29] We also explored the compatibility of CGenFF with VB, and the results are presented in the SI.

In the present work we apply VB for d^6-piano stool complexes which primarily involves the description of the metal interacting with the piano stool moiety. For this, a range of typical piano stool complexes is parametrized within the VB framework, and structural and dynamical properties are determined. Several parametrization strategies are pursued, compared, and validated vis-a-vis existing experimental data (structural and dynamical). However, a full parametrization of every complex, which is outside the scope of the present work, was not attempted. This applies in particular for the nonbonded

Table 1. RMSD of the crystal structure vs. the optimized structures by DFT, CHARMM and VB. RMSD5 includes only the metal, its three bonded neighbor atoms and the dummy atom. The RMSD includes all atoms except hydrogens. Individual RMSDs are given for Mulliken charges, and an overall comparison for all complexes with ChelpG and ESP charges is also reported

			RMSD5 [Å]					RMSD [Å]				
	metal	crystal structure	DFT	VB_{sp^3}	VB_{LC}	C-VB_{LC}	CHARMM	DFT	VB_{sp^3}	VB_{LC}	C-VB_{LC}	CHARMM
1	Ir		–[a]	0.24	0.08	0.08	0.10	–[a]	0.18	0.09	0.08	0.11
2	Ru		–[a]	0.20	0.07	0.07	0.20	–[a]	0.14	0.05	0.05	0.15
3	Rh		–[a]	0.29	0.08	0.08	0.14	–[a]	0.28	0.20	0.20	0.23
4	Ir	CSD: YOBFUR[40]	0.06	0.10	0.11	0.10	0.12	0.41	0.38	0.29	0.39	0.47
5	Rh	CSD: KIMQAY[38]	0.07	0.23	0.12	0.12	0.12	0.59	0.54	0.58	0.53	0.51
5	Rh	CSD: WOLCOP[39]	0.07	0.23	0.11	0.11	0.11	0.60	0.55	0.59	0.54	0.52
6	Ru	CSD: TAXFON[41]	0.07	0.18	0.08	0.08	0.11	0.21	0.44	0.29	0.27	0.30
7	Ru	CSD: ZESSAR[42]	0.07	0.27	0.14	0.15	0.12	0.45	0.60	0.34	0.34	0.31
8	Ir	ref 43	0.06	0.25	0.07	0.06	0.11	0.47	0.36	0.12	0.34	0.33
9	Ir	CSD: ECUBEJ[44]	0.08	0.20	0.09	0.09	0.09	0.52	0.23	0.15	0.17	0.17
10	Ir	ref 45	0.10	0.20	0.12	0.11	0.09	0.26	0.23	0.17	0.22	0.24
11	Ru	CSD: BUCLOB[46]	0.09	0.17	0.07	–[b]	–[b]	0.25	0.32	0.26	–[b]	–[b]
12	Ir	CSD: XUDMUE[47]	0.08	0.23	0.08	0.07	0.13	0.40	0.39	0.41	0.27	0.34
13	Ru	PDB: 2BZH[2]	0.07	0.12	0.09	–[b]	–[b]	0.11	0.29	0.16	–[b]	–[b]
avg. RMSD vs X-ray[c]			0.07	0.20	0.10	0.10	0.11	0.39	0.39	0.30	0.34	0.36
avg. RMSD vs X-ray ChelpG[c]			–	0.24	0.10	0.10	0.14	–	0.42	0.34	0.38	0.42
avg. RMSD vs X-ray ESP[c]			–	0.26	0.11	0.11	0.17	–	0.42	0.31	0.37	0.43

[a]The RMSD and RMSD5 was determined between the DFT and the FF structures. [b]The calculations were performed only using VB. [c]Excluding complexes **1**–**3**.

interactions. Rather, the work focuses on the feasibility of atomistic simulations for d^6-piano stool complexes within a typical parametrization framework which will need to be refined for specialized applications.

COMPUTATIONAL METHODS

Molecular mechanics simulations were carried out in CHARMM[5] using the CHARMM22[30] force field with custom parameters. Further simulations were performed in CHARMM supplemented with the VB module.[19] Electronic structure calculations at the DFT[31] level were carried out with Gaussian.[32] Prototypical three-legged piano stool structures were extracted either from publications, the Cambridge Structural Database (CSD),[33] or the Protein Data Bank (PDB).[34]

Reference Compounds and Reference Calculations. With the aim of modeling important intermediates present in catalytic cycles as well as three-legged piano stool complexes acting as enzyme inhibitors, we selected (η^n-arene)Ru(II)L_3 (n = 5,6) and (η^5-Cp*)M(III)L_3, (M = Ir, Rh) complexes. A representative palette of ancillary ligands L was selected: *N*-heterocyclic carbene, phosphine, diimine, phenylpyridine, amine, aminosulfonamide, aminoalcohol, carbon monoxide, water, chloride, and hydride. All arene caps discussed in this study are planar, i.e., sp^2 hybridized. However, potential distortions from planarity in other structures can be modeled by introducing dihedral terms.

In order to derive the corresponding force field parameters, the 13 three-legged piano stool complexes were subjected to DFT calculations to compute their ground-state geometry and corresponding energy surface scans along specific internal coordinates. The studied complexes are summarized in Figure 1. Calculations were carried out using Gaussian and the hybrid B3LYP functional.[35,36] The atomic basis sets consisted of an effective core potential (LanL2DZ[37]) for the metal and the explicit 6-31G(d,p) basis for all remaining atoms. The quality of the DFT geometries was assessed by computing the RMSD vs the experimental X-ray structures (see Table 1) where available. For complex **5**, two enantiomers were structurally determined[38,39] and thus included.

Force Fields and Parametrization. The standard procedure for deriving CHARMM-parameters uses calculations at the MP2/6-31G(d) level.[27,30] However, as calculations involving transition metals are computationally demanding, we decided to use DFT as reference calculations. One should note that irrespective of the electronic structure level chosen, parameters need to be refined by fitting to experimental data. In particular, parametrization of the nonbonded parameters may be carried out in various ways, ranging from a sequential to a fully combined fit of the nonbonded terms[48] and including experimental data of different origin.[49]

Piano Stool Moiety. In order to describe the three-legged piano stool geometry, all donor atoms of the ligands were explicitly connected to the metal using a bond. For the (η^n-arene)M interaction (n = 5,6) a dummy atom X at the barycenter of the ring was introduced.[50] It was incorporated in CHARMM and VB using the lonepair module and thus kept at the center of the ring throughout the simulation. In order to maintain an sp^2 hybridization of the arene carbons, no explicit bond between the dummy atom and the arene carbons was introduced. To account for the tilting of the ring, M–X–C_{arene} angles were included. The M–C_{arene} van der Waals (vdW) and electrostatic interactions were excluded to avoid redundant counting of interactions already present in the M–X bond. Dihedral terms in metal complexes are generally neglected[18] which was also done here. The following force field combinations were considered in more detail.

Pure VB:VB_{sp^3} Model. According to VB, all piano stool complexes would be hypervalent. However, by introducing a dummy atom as a point of reference for the arene, the hypervalency concept no longer applies, as the bond between the dummy atom and the metal accounts for more than two

electrons. Thus we decided to work within nonhypervalent VB by using $sp^m d^n$ hybridizations. In light of the $(\eta^n$-arene$)M(L)_3$ structure, reminiscent of a tetrahedron, the tetrahedral sp^3 hybridization was shown to be a good starting point to optimize the geometry of the three-legged piano stool.

Pure VB:VB$_{LC}$ Model. As angles observed in X-ray structures tend to cluster around 90° (between the piano stool legs) or 130° (between the ring-center and the piano stool legs), the tetrahedral approximation with its canonical 109.5° angles is not optimal. Instead, a linear combination of other hybridizations can be envisaged. As shown in Figure 2, the angle-dependent VB-energy for sp^3d^2 has a minimum at 90°, whereas for sp^3d^5 its minimum is at 130°. Therefore sp^3d^2 was used as hybridization of the piano stool leg orbitals, whereas the hybridization for the M−X orbital was sp^3d^5. Such orbitals have been used to describe OC−M−CO angles previously,[51] but their use here is empirical, as a combination sp^3d^2 and sp^3d^5 hybridizations is used on the metal.

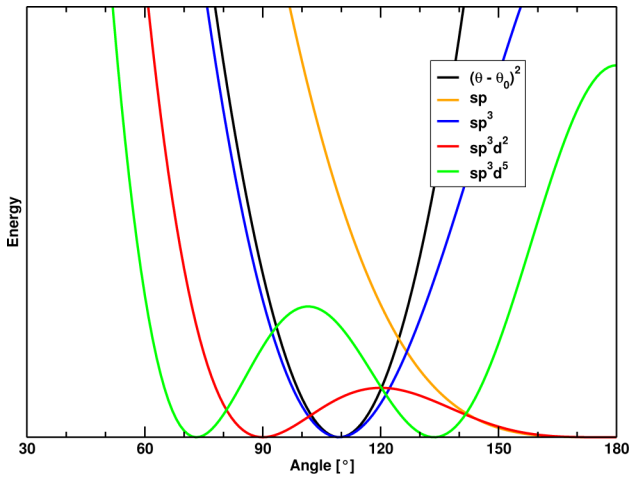

Figure 2. VB energy (no scale given) as a function of the angle for several hybridizations. For comparison, the energy function of a harmonic angle with θ_0 = 109.5° is shown as well.

Standard CHARMM. All angles are treated with standard CHARMM, no VB is in use.

Mixed CHARMM/VB:C-VB$_{LC}$ Model. A mixed VB and CHARMM potential energy function whereby a VB-energy term is combined with conventional CHARMM angle terms. Only the X−M−L and L−M−L angles surrounding the metal are treated by VB, whereas all other angles are calculated with CHARMM.

Parametrization. Force field parametrization was carried out by fitting the parameters to reproduce the energy profiles of energy surface scans obtained from DFT calculations. Parameters not available in the standard CHARMM22 force field were those either derived previously[52] or taken from parameters for related chemistries through analogies. The fitting was performed using the full force field as opposed fitting the respective parameter without other terms involved. To assist parametrization, perl scripts from PerlMol (www.perlmol.org) were used to generate the topology and necessary input files for the CHARMM calculations directly from the Gaussian output files. The fitting itself was performed using Chnolls,[49] the CHARMM interface for Inolls.[53] For the charges of the ligand atoms, Mulliken charges from the DFT optimizations were used and not specifically optimized. To assess the influence of the charge scheme used for these complexes, we also tested ChelpG[54] and ESP[55,56] charges, and the results are reported in Tables 1 and S3. It is worthwhile to mention that full compatibility with CHARMM would require fitting nonbonded parameters to interaction energies with a water molecule. No such full parametrization was attempted in the present case which, however, would be certainly possible and necessary for specific applications. vdW parameters for all atoms except for the metal were those from the CHARMM22 force field, whereas for the metal atoms those from UFF[57] were used. As CHARMM and UFF use different mixing rules[58] this could certainly be improved. However, for all complexes studied here, the metal is buried by the ligands and vdW contact with, e.g., the surrounding solvent is minor (see also Figures 8 and 9). A flowchart summarizing the parametrization is presented in Figure 3. To validate the procedure, the bidentate ligands present in complexes **6** and **9** were also parametrized by using CGenFF[27] for the ligands within models VB$_{LC}$ and VB$_{sp^3}$ models. The corresponding results are reported in Table S3.

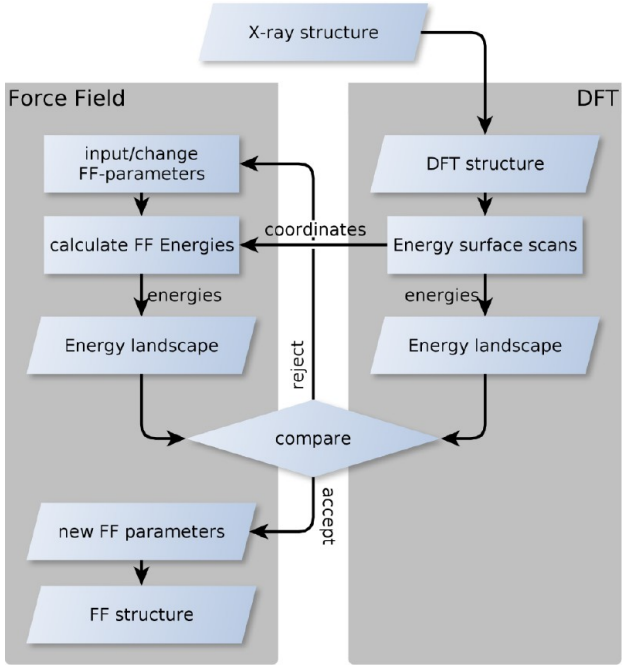

Figure 3. Summary of the force field parametrization procedure.

All VB parameters were set to the default[22−24] ones except for the scaling parameter k_{Ru-N} which is 100 kcal/mol for VB$_{sp^3}$. For the more comprehensive VB$_{LC}$ model, the scaling parameters $k_{metal-ligand}$ were refitted where necessary. All bond and angle parameters were fitted or assigned, and only a small number of dihedral terms was required to obtain satisfactory results. The recommended CHARMM22 cutoffs and settings[30] were used in the parametrizations and simulations: a switching (vdW terms) respectively shifting (electrostatics) function between 10 and 12 Å, cutoffs at 12 Å, and atom-based electrostatics.

Force Field Calculations. *Structure Optimization.* Of the 13 complexes that were considered, 10 have been structurally characterized by experiment. First, the structures of all complexes were optimized with DFT and with CHARMM and VB using the conjugate gradient method until convergence

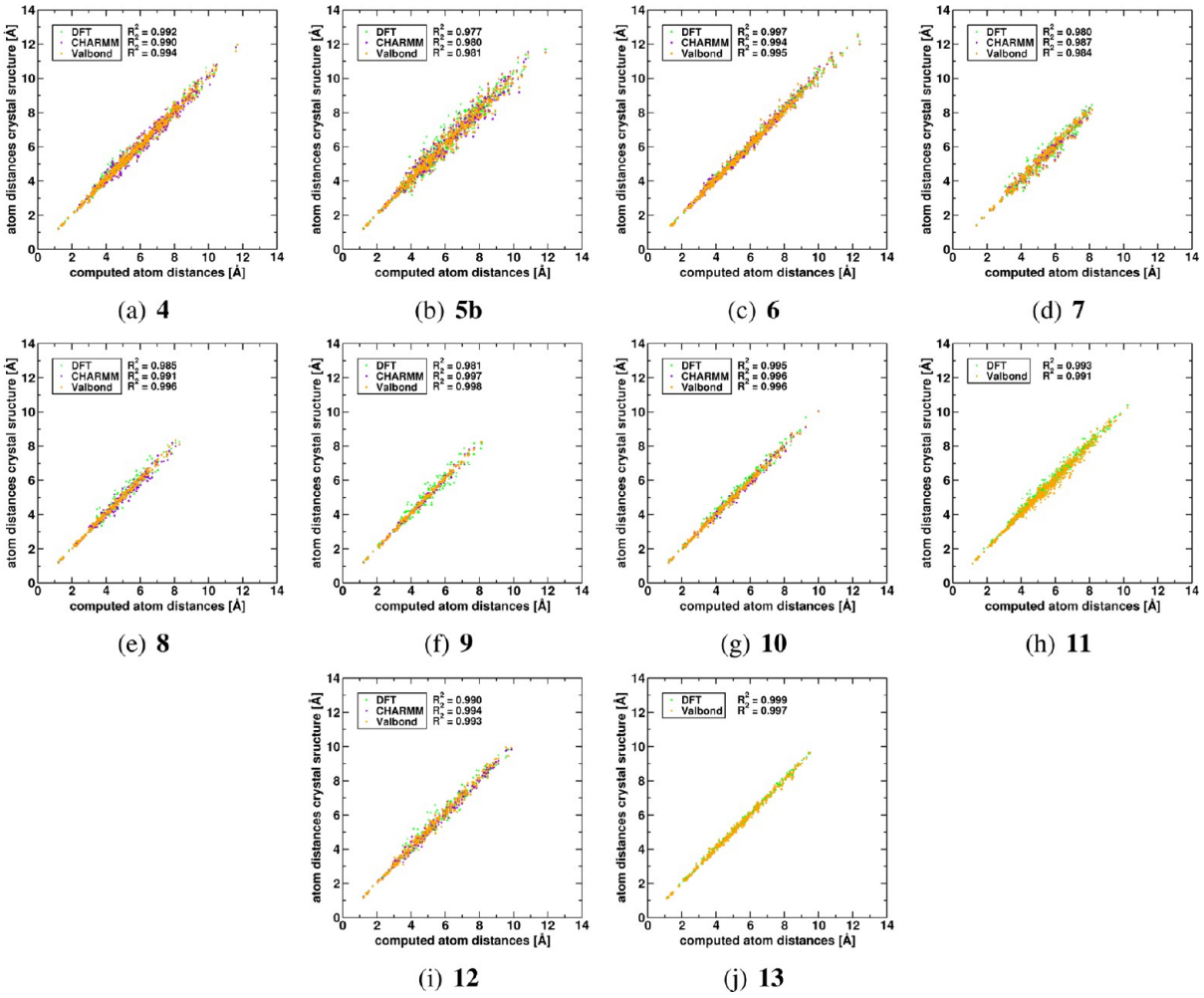

Figure 4. Comparison of the atom distances in the crystal (*y*-axis) and the calculated (*x*-axis) structures. Values for the distances in the DFT-optimized structures are displayed in green, for the CHARMM optimized structures in purple and in the VB optimized structures (VB_{LC} model) in orange.

($\Delta E < 10^{-5}$ kcal/mol) was achieved. The structures were then compared by calculating the RMSD between X-ray and the energy minimized structures for all atoms except hydrogens (RMSD) and for the five "core atoms" (i.e., the three donor atoms, the dummy atom, and the metal, RMSD5), respectively. In addition, the complete distance matrix between pairs of heavy atoms was determined from the reference and computationally optimized structures.

MD Simulation in the Gas Phase. For selected complexes, molecular dynamics (MD) simulations with each of the computational models (VB_{sp^3}, VB_{LC}, CHARMM, and C-VB_{LC}) were performed. An initial 10 ps (with a stepsize of Δt = 0.2 fs) heating period from 100 to 300 K was followed by 20 ps of equilibration at 300 K. No SHAKE[59] was used. Following this, 2 ns trajectories in the NVE (microcanonical) ensemble were run to assess the stability of the simulations. All simulation conditions were identical to those used for the minimizations. As demonstrated previously,[60] VB simulations can be carried out on the 100 ns time scale. However, for the purpose of the present work (validation of energy conservation), this was not deemed necessary.

Explicit Solvent Simulations. For molecule **1**, MD simulations with CHARMM in explicit solvent were performed in two different solvents. The VB_{LC} approach in combination with standard CHARMM was chosen to perform these simulations to illustrate the interplay of the VB force field with conventional CHARMM. VB was only used for the metal complex, and the solvents were treated with conventional CHARMM. The first simulation was carried out in explicit water (TIP3P model).[61] The second simulation was performed in a methanol solvent box using parameters from the CHARMM22 force field. The simulations were done with periodic boundary conditions in a cubic solvent box of 32 Å (methanol) or 35 Å (water) edge length. A time step of 1 fs was used. SHAKE[59] was employed on the bonds involving hydrogen atoms. After heating and equilibration, simulations were done in the NPT ensemble, keeping pressure and temperature constant with the extended system thermostat.[62−64] A total of 5 ns were simulated for the complex with each of the solvents. Cutoffs and remaining settings were identical as above.

NMR Calculations. To further validate the parametrizations against solution-phase data, chemical shifts for complex **9** were determined. Two simulations in explicit water for complex **9** were carried out: one using the same conditions as above and a second simulation without employing SHAKE for the hydrogens of the metal complex. The ^{1}H and ^{13}C chemical shifts were calculated for both the DFT-optimized structures and the

500 snapshots from the MD simulations using the gauge-independent atomic orbital (GIAO) method.[65] From the 500 snapshots, a "spectrum" was generated by calculating the distribution of the chemical shifts in the snapshots. Two functionals were used, namely the standard B3LYP and the dispersion corrected M06-2X functionals.[66]

RESULTS AND DISCUSSION

Reference Compounds, Reference Calculations, and Parametrization. The largest RMSD between the X-ray and the DFT-optimized structures for the five "core atoms" (RMSD5) is 0.10 Å (see Table 1), demonstrating that DFT calculations are well suited to reproduce ground-state piano stool geometries. The influence of the charge models used in the parametrization (Mulliken, ChelpG, and ESP) on describing the structural data was found to be rather small. The RMSD5 is virtually the same for all charge models, the RMSD is slightly smaller with the Mulliken charges. Typically, the charges differed by less than 0.1 *e*. But for the metal charges, deviations of up to 0.4 *e* were observed. The distance matrices (Figure 4) correlate well with X-ray geometries (R^2 = 0.98−0.99).

In a next step, the bonded parameters (bond, angles) of the force field were parametrized. For this purpose, energy surface scans were carried out for complexes **1**−**3**, **7**, and **10**−**12** along different relevant internal coordinates. The bonds scanned are summarized in Table 2, and the list of scanned angles is collected in the SI. The force field parameters were optimized by using the Chnolls platform as described above to minimize the difference in energy between the force field and DFT energy landscapes. Relevant optimized bond parameters and refitted VB scaling factors are collected in Table 2. A complete list of all parameters in CHARMM format is collected in the SI as are the topology files for all complexes.

Table 2. M−L Bond Length Parameters and VB Orbital Scaling Parameters[a]

		bond parameters		VB parameter	
atoms		force constant kcal/mol/Å^2	equilibrium Å	scaling factor[b] kcal/mol	fitting on structure
Ru	X	210	1.72	140	**2**
Ru	N	113	2.28	500	**2**
Ru	Cl	105	2.50	350	**2**
Ru	$C_{carbene}$	106	2.05	100[c]	**11**
Ru	C_{CO}	206	1.80	100[c]	**11**
Ru	H	138	1.54	100[c]	**11**
Ru	P	62	2.08	100[c]	**7**
Rh	X	210	1.81	100[d]	**3**
Rh	N	70	2.38	285[d]	**3**
Rh	Cl	77	2.54	260[d]	**3**
Ir	X	210	1.81	100	**1**
Ir	N	100	2.30	285	**1**
Ir	Cl	113	2.50	260	**1**
Ir	O	145	2.11	250	**12**
Ir	C	130	2.00	100[c]	**10**

[a]Equilibrium parameters are not necessarily identical to the bond length found in X-ray structures, as the parameters are fitted to reproduce energy surface scans and not minimum-energy structures. [b]Only for the VB_{LC} model, default[22−24] values for VB_{sp^3} model. [c]Default value, not fitted. [d]Fitted for iridium.

For the VB_{sp^3} model, only one VB parameter (k_{Ru-N}) needed to be adapted for accurately reproducing the minimum-energy structures for the 13 molecules. All other VB parameters could be kept at their default values, and no further adjustments were necessary, thus considerably reducing the amount of reparametrization required. For the more elaborate model with the linear combination of hybridizations (VB_{LC}), seven parameters were refitted. In comparison, more than 200 nonstandard CHARMM angle parameters were parametrized or assigned by analogy, even though we reduced the test set for CHARMM to only 11 from the original 13 molecules. Including complexes **11** and **13** would require an additional 40 terms to be determined.

Force Field Calculations. *Structure Optimization.* In order to estimate the quality of the force field-calculated structures for complexes **4**−**13**, RMSD and RMSD5 relative to the X-ray structures were calculated. For model complexes where no X-ray data are available (complexes **1**−**3**), the RMSD were computed relative to the DFT-optimized structures. RMSD5 for the VB_{sp^3} model is slightly higher compared to the DFT optimized structures (Table 1). In contrast, the RMSD for the entire structures (excluding hydrogens) is comparable or even smaller than that for the DFT structures. The average RMSD vs X-ray is the same for DFT and the VB_{sp^3} model (0.39 Å), whereas the average RMSD5 for the VB_{LC} model, the CHARMM-only parametrization and the C-VB_{LC} model is virtually the same. The average global RMSD for these three cases is slightly lower than for DFT, with VB_{LC} performing best. As expected, the results for the two enantiomers of complex **5** are very similar. Distance matrices show a similar trend (Figure 4) with deviations for the force fields slightly smaller than for the DFT calculations. For comparison, all superimposed structures are presented in Figure 5. As can be appreciated, the force field and DFT-calculated structures are strikingly similar to the X-ray structures. The largest deviations arise from rotations of aromatic residues in the second coordination sphere of the metal. Crystal contacts in the X-ray structures might be responsible for this, and improvements may be possible by introducing additional dihedral angle parameters. The VB optimized structures for complexes **11** and **13** yield a nonlinear M−C−O arrangement (α = 160°) with tilting of the C−O toward the η^n arene moiety. This may be a limitation in the VB approach as the energy surface for sp hybridizations is very flat (see Figure 2), and thus the distortion of the angle from 180° is not hindered enough by the force field. This issue was resolved by adding a small (10 kcal/mol) harmonic constraint around 180°.

A 72° rotation of the *Cp** ring results in a structure which is energetically and structurally indistinguishable (Figure 6). To evaluate the torsional barrier of the *Cp** rotation, a potential surface scan for the rotation along the *Cp**−Ir bond was performed on complex **1** at the DFT level. The maximal energy variation was found to be <0.2 kcal/mol with a quasiperiodicity of 72° (Figure 6).

The four models differ in number and types of parameters needed. VB_{sp^3} is straightforward and required least parametrization. The results are robust and valid for exploratory simulations, although with the present parametrizations it shows the largest deviations. The VB_{LC} model required reparametrization of several VB parameters, and the results are meaningful. The CHARMM approach involves most parametrization, and the results are slightly worse for the angles involving metals. Using the C-VB_{LC} model is a compromise between the CHARMM and the VB force field,

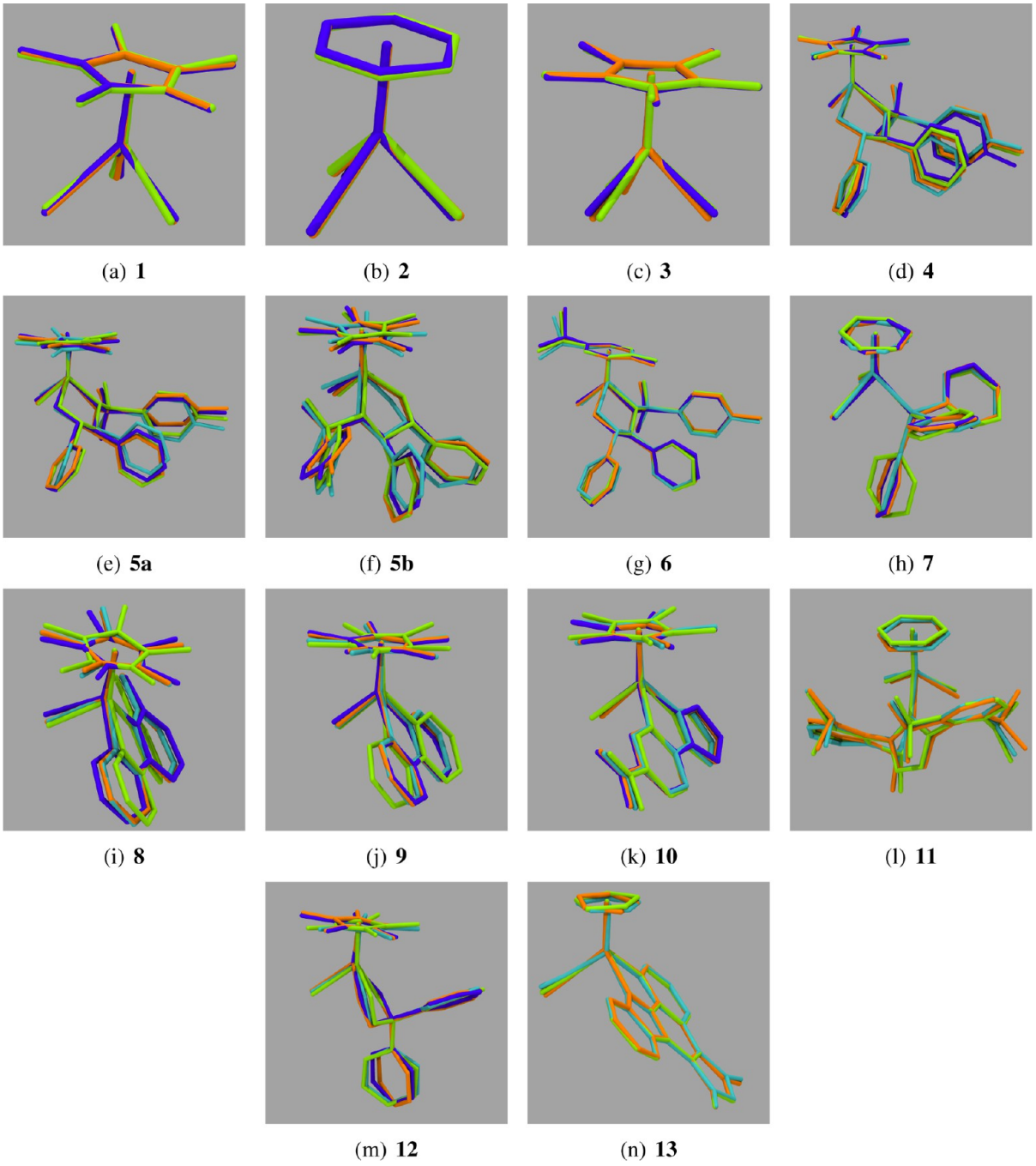

Figure 5. Superposition of the crystal structure (cyan) with the DFT-optimized (green), the CHARMM optimized (purple) and the VB optimized (VB_{LC} model, orange) structures. The superposition minimizes the RMSD.

and VB is only used for the L−M−L angles. As the L−M−L angles are best described by VB and given that reliable CHARMM parameters for the ligands are available, e.g., through parametrization with CGenFF, we recommend the C-VB_{LC} as the default approach for production simulations. If no parameters are readily available, we recommend the VB_{LC} model. For all these models it should be emphasized that depending on the purpose, further reparametrization in particular of the nonbonded parameters may be required. Also, the merits and disadvantages of the four models explored here may be more or less accentuated if such a more complete parametrization is carried out.

MD in Gas Phase. To verify that the forces were correctly implemented and to demonstrate the capability of following explicit dynamics of a system in a representative environment, MD simulations were performed. Because the resulting trajectories all display similar behavior of the complexes, we focused on simulations of molecules **1** and **4** using the VB_{LC} approach for a more detailed analysis.

The total energy is conserved during the 2 ns NVE VB MD simulation and the temperature as well as the kinetic and potential energies are Gaussian distributed as expected, see Figure S4. For the RMSD of all atoms except hydrogens (RMSD), several stable states can be identified (see Figure 7). Each of these corresponds to a 72° rotation of the *Cp** moiety

dx.doi.org/10.1021/ct301080d | *J. Chem. Theory Comput.* 2013, 9, 2313−2323

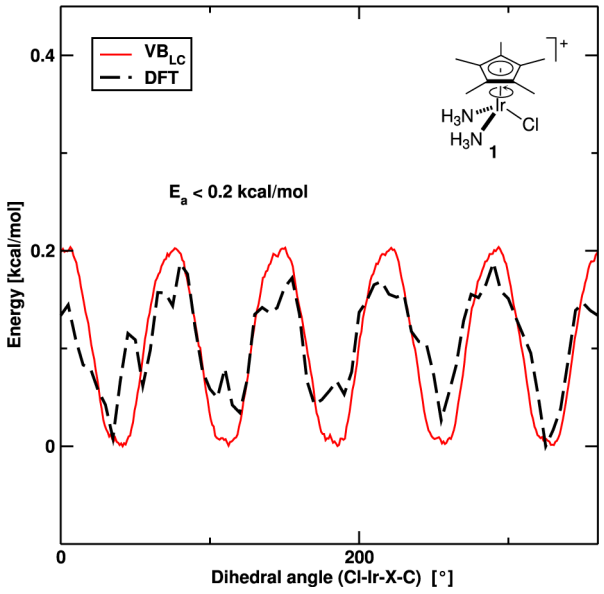

Figure 6. Computed energy profile for the rotation of *Cp** around the X−Ir axis in complex **1**. (Black dashed line is the DFT energy. Red line is the energy according to probability distribution of the dihedral angle for the MD simulation with the VB_{LC} model.).

along the X−Ir axis and illustrates the low activation energy required for an M−*Cp** rotation. The probability distribution of the dihedral angle Cl−Ir−X−C results in an energy barrier of 1.5 kcal/mol for complex **4**. For complex **1** it yields 0.2 kcal/mol, reproducing ΔE calculated using DFT with remarkable accuracy (see Figure 6). According to transition-state theory, $1/\tau_{A\rightarrow B} = (k_b T/h)\exp(-\Delta G_{A\rightarrow B}/k_b T)$, the states have lifetimes on the ps time scale which can be confirmed by visual analysis of the rotation where the lifetime of the states is ≈10 ps for complex **4** and ≈1 ps for complex **1**, respectively.

At t = 1.6 ns one of the phenyl rings of the sulfonamide ligands flips, resulting in the observed increase of the RMSD. The RMSD5 remains <0.3 Å, and no drift can be observed. For several hundred snapshots energy calculations using DFT and the C-VB_{LC} force field have been carried out. The correlation between force field and DFT calculations is R = 0.8. This is an acceptable correlation but could be further improved by refitting the nonbonded parameters which, however, is outside the scope of the present work. The results demonstrate that robust NVE simulations are possible which opens the way for more elaborate investigations. As reported in Table S3, the results from calculations based on the CGenFF parametrizations were similar to simulations using our parameters (slightly worse results for complex **9** and slightly better results for complex **6**), which illustrates the robustness of the present approach.

Explicit Solvent Simulations. For organometallic complexes, the dynamics in a realistic solvent environment is of particular interest because additional factors influencing their activity and behavior arise. They include direct solvent coordination, electrostatic shielding, and entropic effects and can affect conformations and reactivities of the chemical species involved. Often, such effects are excluded or only taken into account in a highly averaged fashion in computational investigations of transition-metal compounds because a realistic solvent environment increases the number of atoms by at least an order of magnitude and renders such studies impractical. In the following, we consider the organization of solvent molecules around complex **1** in two different solvents as an example.

The RMSD over the duration of the simulations in explicit solvent behave similarly to simulations in the gas phase. Simulations in water or methanol do not significantly differ. To investigate the effects of the solvent on the simulation, i.e., the solvation shell, the solvent distribution around the metal complex during the simulation was characterized. The solvent is represented as a density map for each element type, see Figures

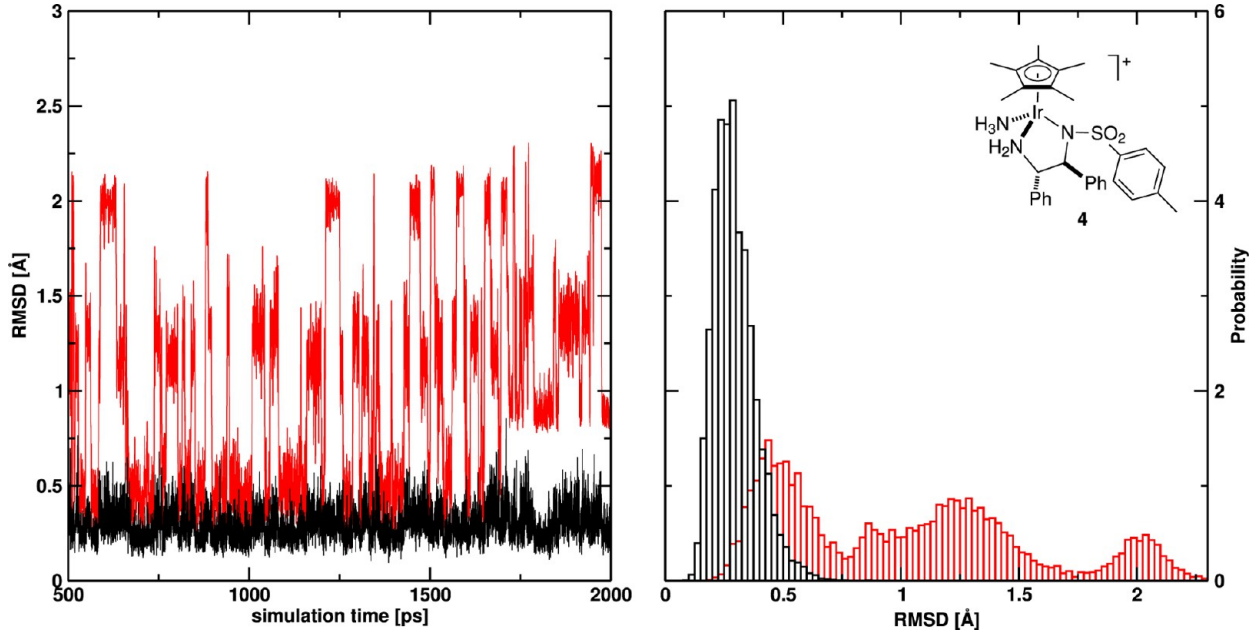

Figure 7. RMSD during the MD simulation using VB_{LC} for complex **4**. For the 5 core atoms (black traces), the RMSD remains <0.5 Å during most of the simulation. Inclusion of all heavy atoms (red traces) reveals higher deviations diagnostic of the rotation of the *Cp** moiety along the M−*Cp** axis.

dx.doi.org/10.1021/ct301080d | *J. Chem. Theory Comput.* 2013, 9, 2313−2323

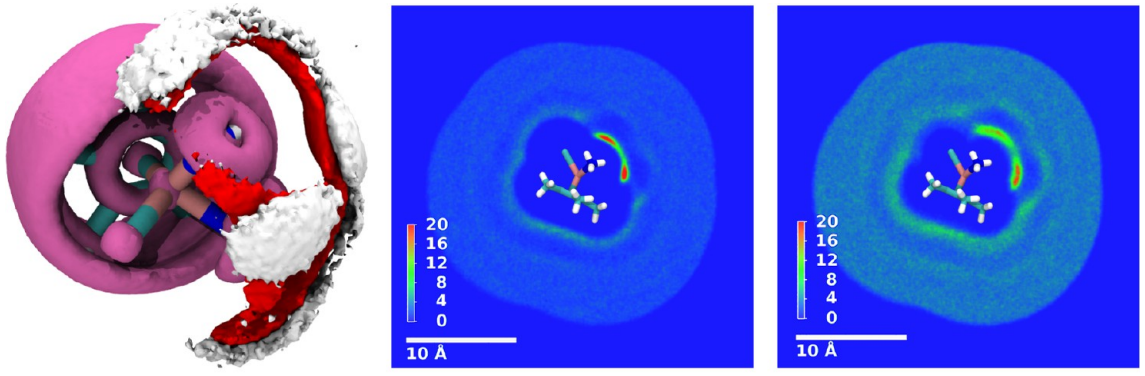

(a) (b) **Oxygen** (c) **Hydrogen**

Figure 8. Solvent distribution for an MD simulation of complex **1** in explicit water. (a) 3D representation of the atom distribution around the metal complex during the simulation. The probability density for the piano stool atoms is colored in magenta, whereas for the solvent atoms it is depicted as separate densities for each element (oxygens, red; hydrogens, white). The isosurfaces are drawn at 5%, 30%, and 40% of the maximum density for the metal complex, the water−oxygens and the water−hydrogens, respectively. (b) and (c) Slice through the probability distribution for oxygens (b) and hydrogens respectively (c) for the duration of the simulation with a cutoff of 10 Å around the complex. The slice was cut through the plane formed by the metal, the dummy atom, and the chloride. The scale in (b) and (c) reports total counts in voxels of size 0.2 × 0.2 × 0.2 $Å^3$.

8a and 9a. Each snapshot is oriented such as to minimize RMSD5 and thus remove the translational and rotational degrees of freedom.

The resulting density for the metal-complex atoms shows the rotation of the *Cp** ring for both solvents. It also reveals only very little movement of the metal-connecting atoms. Slices through these density maps are displayed in Figures 8 and 9 for water and methanol, respectively. The density was cut through the mirror plane formed by the M−X−Cl plane, slicing the complex into two mirror images. The oxygen-atom density in both cases (water and methanol) is highest next to the ammonia hydrogens, a result of the polar interactions. A first and a second solvation shell with a region of lower probability in between can clearly be identified. The carbon density is highest on top of the *Cp** ring highlighting the hydrophobicity of the *Cp** moiety. The high densities close to the ammonia groups result from orientation of the methanol molecules to present the oxygen toward the hydrogens. The hydrogen atom densities concur with the observations made for the carbon and oxygen atoms. In regions where the heavy-atom densities are highest, the solvent molecules are more ordered, and thus the hydrogen densities are more localized as well. Overall, ordering is dominated by hydrophilic rather than hydrophobic interactions as the respective solvent densities are more influenced by the higher charged nitrogen than the less charged carbon atoms of the ligand.

The configurations sampled can also be used to further assess the force field parametrization. We stress again, that no attempt was made to further refine the nonbonded parameters to optimally reproduce reference electronic structure calculations, as such quantitative studies are not the focus of the present work. This can in principle done using available tools.[49] Rather, an ensemble of 1000 complex:solvent structures including the complex with **1** and **3** nearby water molecules were extracted from the simulations and their stabilization energies were computed from VB_{LC} and DFT (B3LYP and M06-2X functional with basis sets as described above) electronic structure calculations. A graphical comparison of the two methods is provided in Figure S5, and the correlation coefficients are R = 0.62 and 0.66, respectively.

NMR Calculations. In order to assess the suitability of such simulations in solution, NMR chemical shifts from explicitly solvated simulations in H_2O were determined for complex **9**. Figure S6 compares the experimentally determined shifts[44] with those computed for the DFT-optimized structures and the conformationally averaged shifts. The experimental values were determined in D_2O at 298 K. For the ^1H chemical shifts, surprisingly, the DFT B3LYP calculation performs better than the dispersion-corrected M06-2X functional. MD simulations lead to significant broadening of the peaks due to conformational sampling. This is particularly evident for simulations without SHAKE as the hydrogen bonds are allowed to fluctuate. However, the maxima of the distributions match the experimentally determined chemical shifts quite well. A recent parametrization of sulfonyl containing compounds[67] also used NMR data but in a somewhat more qualitative fashion to validate the parametrizations. In line with the present work, the distributions of the geometrical coordinates used to make contact with the experimentally observed chemical shifts are broad. The present comparison suggests that the force field parameters are a useful starting point but also that there is room for improvement should the particular application require that.

■ CONCLUSIONS

Parameters, suitable for atomistic simulations of d^6 three-legged piano stool complexes with the VB and the CHARMM force field, have been developed and tested for minimum-energy structures and explicit simulations. Specifically, (η^n-arene)ML_3 (n = 5,6) complexes with ruthenium, rhodium and iridium metals and with N-heterocyclic carbene, phosphine, diimine, phenylpyridine, amine, aminosulfonamide, aminoalcohol, carbon monoxide, water, chloride, and hydride as ligands were parametrized. With these parametrizations the complexes can be treated either using the traditional CHARMM or the VB extended CHARMM force fields. From a parametrization perspective, the VB force field is advantageous, as it requires fewer parameters. Specifically, only bonded parameters need to be parametrized, the default VB angle parameters[22−24] with Mulliken charges and vdW parameters from the UFF force field yield meaningful results thus considerably reducing the

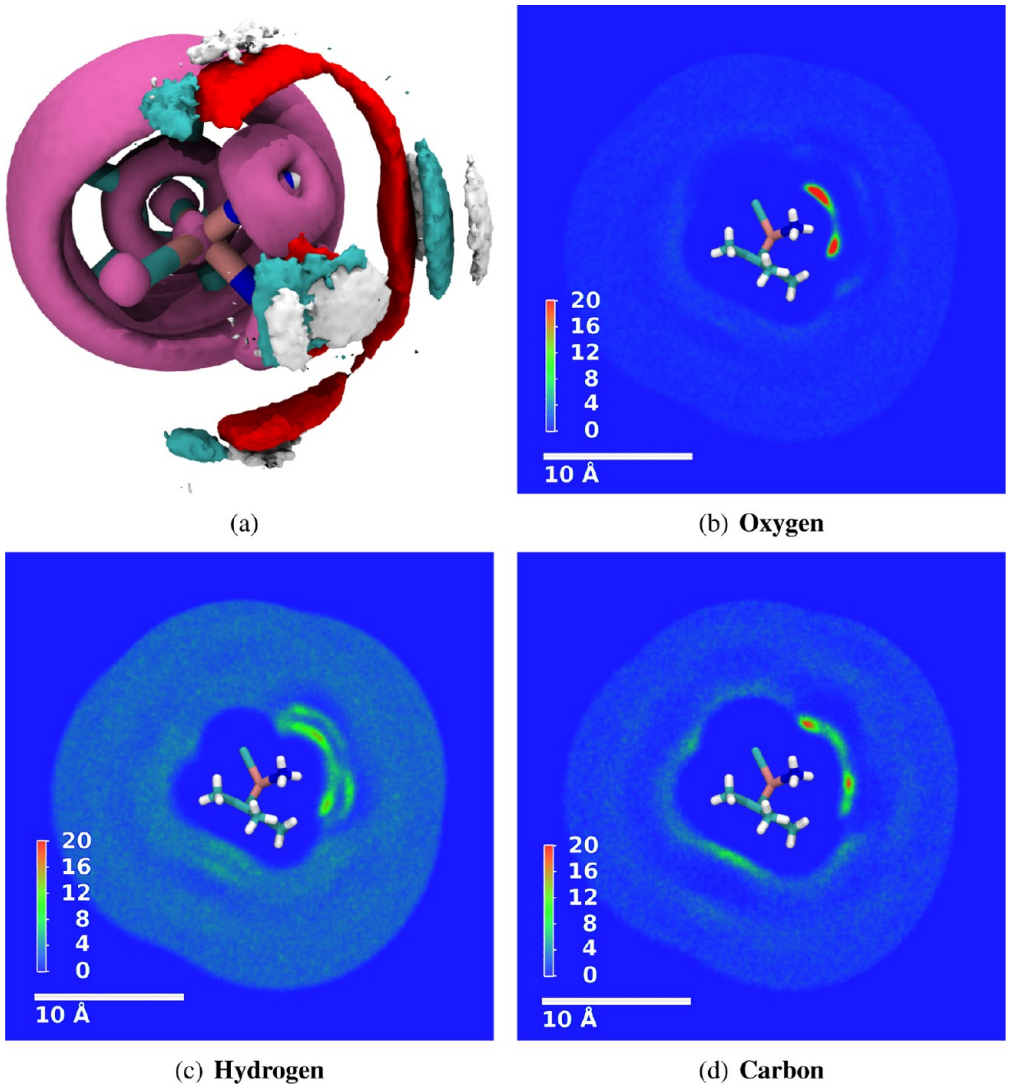

Figure 9. Solvent distribution for an MD simulation of complex **1** including explicit methanol. (a) 3D representation of the atom distribution around the metal complex during the simulation. The probability density for the piano stool atoms is colored in magenta, whereas for the solvent atoms it is depicted as separate densities for each element (oxygens, red; hydrogens, white; and carbons, cyan). The isosurfaces are drawn at 5%, 30%, and 40% of the maximum density for the metal complex, the water−oxygens and the water−hydrogens, respectively. (b−d) Slice through the probability distribution for oxygens (b), hydrogens (c), and carbons (d), respectively, for the duration of the simulation with a cutoff of 10 Å around the complex. The slice was cut through the plane formed by the metal, the dummy atom, and the chloride. The scale in (b−d) reports total counts in voxels of size 0.2 × 0.2 × 0.2 Å^3.

parametrization effort. As VB is compatible with the traditional CHARMM angular parameters, mixed VB/CHARMM calculations can be performed to combine the strengths of both approaches: the established quality of CHARMM for simulations of large biomolecules and the versatility of VB for unusual geometries of metal complexes.

The present work establishes that geometrical structures can be reliably reproduced compared to X-ray and DFT structures, respectively. The RMSDs between X-ray and structures for the four models are comparable to RMSDs obtained between X-ray and DFT structures. Extensive MD simulations are possible which allows, in principle, to investigate the solvent structure around the organometallic complex and capture effects, such as entropy changes upon binding. However, for specific catalysts and depending on the concrete application, further refinement, e.g., by fitting to vibrational or thermodynamic data, of the force field will be necessary. The techniques presented here will be useful starting points for investigating catalysts in dynamically more demanding environments, including their roles in artificial metalloenzymes and as enzyme inhibitors.

■ ASSOCIATED CONTENT

Supporting Information

Force field parameters, topology files, an example input file, additional tables (list of scanned L−M−L angles, metal distances and comparison to CGenFF) and figures (describing the fitted PES, metal distances, the correlation between DFT and FF energies for complexes with water, a comparison of calculated and experimental chemical shifts, and energy distribution during the simulation). This material is available free of charge via the Internet at http://pubs.acs.org.

■ AUTHOR INFORMATION

Corresponding Author

*E-mail: thomas.ward@unibas.ch; m.meuwly@unibas.ch

Notes

The authors declare no competing financial interest.

■ ACKNOWLEDGMENTS

This work was financially supported by the Schweizerischer Nationalfonds through projects PDFMP2 127457 and 200021-117810.

■ REFERENCES

(1) Murata, K.; Ikariya, T.; Noyori, R. *J. Org. Chem.* **1999**, *64*, 2186−2187.
(2) Debreczeni, J. E.; Bullock, A. N.; Atilla, G. E.; Williams, D. S.; Bregman, H.; Knapp, S.; Meggers, E. *Angew. Chem., Int. Ed.* **2006**, *45*, 1580−1585.
(3) Zimbron, J. M.; Sardo, A.; Heinisch, T.; Wohlschlager, T.; Gradinaru, J.; Massa, C.; Schirmer, T.; Creus, M.; Ward, T. R. *Chem.—Eur. J.* **2010**, *16*, 12883−12889.
(4) Monnard, F. W.; Heinisch, T.; Nogueira, E. S.; Schirmer, T.; Ward, T. R. *Chem. Commun.* **2011**, *47*, 8238−8240.
(5) Brooks, B. R.; Bruccoleri, R. E.; Olafson, D. J.; States, D. J.; Swaminathan, S.; Karplus, M. *J. Comput. Chem.* **1983**, *4*, 187−217.
(6) Case, D. A. et al. *Amber 12*; University of California, San Francisco: San Francisco, CA, 2012.
(7) Schuler, L. D.; Daura, X.; van Gunsteren, W. F. *J. Comput. Chem.* **2001**, *22*, 1205−1218.
(8) Jorgensen, W. L.; Maxwell, D. S.; Tirado-Rives, J. *J. Comput. Chem.* **1996**, *118*, 11225−11236.
(9) Bosnich, B. *Chem. Soc. Rev.* **1994**, *23*, 387−395.
(10) Polzer, T.; Kiefer, W. *J. Organomet. Chem.* **1996**, *508*, 153−157.
(11) de Hatten, X.; Cournia, Z.; Huc, I.; Smith, J.; Metzler-Nolte, N. *Chem.—Eur. J.* **2007**, *13*, 8139−8152.
(12) Bernhardt, P. V.; Comba, P. *Inorg. Chem.* **1992**, *31*, 2638−2644.
(13) Norrby, P.-O.; Brandt, P. *Coord. Chem. Rev.* **2001**, *212*, 79−109.
(14) Piquemal, J.-P.; Williams-Hubbard, B.; Fey, N.; Deeth, R. J.; Gresh, N.; Giessner-Prettre, C. *J. Comput. Chem.* **2003**, *24*, 1963−1670.
(15) Comba, P.; Hambley, T. W.; Martin, B. *Molecular Modeling of Inorganic Compounds*; Wiley-VCH: Weinheim, Germany, 2009; p 344.
(16) Zimmer, M. *Coord. Chem. Rev.* **2009**, *253*, 817−826.
(17) Deeth, R. J.; Anastasi, A.; Diedrich, C.; Randell, K. *Coord. Chem. Rev.* **2009**, *253*, 795−816.
(18) Hu, L.; Ryde, U. *J. Chem. Theory Comput.* **2011**, *7*, 2452−2463.
(19) Tubert-Brohman, I.; Schmid, M.; Meuwly, M. *J. Chem. Theory Comput.* **2009**, *5*, 530−539.
(20) Boeyens, J. C.; Comba, P. *Coord. Chem. Rev.* **2001**, *212*, 3−10.
(21) Comba, P.; Zimmer, M. *J. Chem. Educ.* **1996**, *73*, 108−110.
(22) Root, D. M.; Landis, C. R.; Cleveland, T. *J. Am. Chem. Soc.* **1993**, *115*, 4201−4209.
(23) Cleveland, T.; Landis, C. R. *J. Am. Chem. Soc.* **1996**, *118*, 6020−6030.
(24) Landis, C. R.; Cleveland, T.; Firman, T. K. *J. Am. Chem. Soc.* **1998**, *120*, 2641−2649.
(25) Pauling, L. *J. Am. Chem. Soc.* **1931**, *53*, 1367−1400.
(26) Landis, C. R.; Cleveland, T.; Firman, T. K. *J. Am. Chem. Soc.* **1995**, *117*, 1859−1860.
(27) Vanommeslaeghe, K.; Hatcher, E.; Acharya, C.; Kundu, S.; Zhong, S.; Shim, J.; Darian, E.; Guvench, O.; Lopes, P.; Vorobyov, I.; Mackerell, A. D. *J. Comput. Chem.* **2010**, *31*, 671−690.
(28) Vanommeslaeghe, K.; MacKerell, a. D. *J. Chem. Inf. Model.* **2012**, *52*, 3144−3154.
(29) Vanommeslaeghe, K.; Raman, E. P.; MacKerell, a. D. *J. Chem. Inf. Model* **2012**, *52*, 3155−3168.
(30) MacKerell, A. D.; et al. *J. Phys. Chem. B* **1998**, *102*, 3586−3616.
(31) Hohenberg, P.; Kohn, W. *Phys. Rev.* **1964**, *136*, B864−B871.
(32) Frisch, M. J. et al. *Gaussian 03*, revision B.01; Gaussian, Inc.: Wallingford, CT, 2006.
(33) Allen, F. H. *Acta Crystallogr., Sect. B: Struct. Sci* **2002**, *58*, 380−388.
(34) Bernstein, F. C.; Koetzle, T. F.; Williams, G. J.; Meyer, E. F.; Brice, M. D.; Rodgers, J. R.; Kennard, O.; Shimanouchi, T.; Tasumi, M. *Arch. Biochem. Biophys.* **1978**, *185*, 584−591.
(35) Becke, A. D. *J. Chem. Phys.* **1993**, *98*, 5648−5652.
(36) Stephens, P. J.; Devlin, F. J.; Chabalowski, C. F.; Frisch, M. J. *J. Phys. Chem.* **1994**, *98*, 11623−11627.
(37) Hay, P. J.; Wadt, W. R. *J. Chem. Phys.* **1985**, *82*, 270−284.
(38) Mashima, K.; Abe, T.; Tani, K. *Chem. Lett.* **1998**, 1199−1200.
(39) Mao, J.; Baker, D. C. *Org. Lett.* **1999**, *1*, 841−843.
(40) Heiden, Z. M.; Gorecki, B. J.; Rauchfuss, T. B. *Organometallics* **2008**, *27*, 1542−1549.
(41) Uematsu, N.; Fujii, A.; Hashiguchi, S.; Ikariya, T.; Noyori, R. *J. Am. Chem. Soc.* **1996**, *118*, 4916−4917.
(42) Elsegood, M. R.; Tocher, D. A. *Polyhedron* **1995**, *14*, 3147−3156.
(43) Fujita, K.-i.; Yoshida, T.; Imori, Y.; Yamaguchi, R. *Org. Lett.* **2011**, *13*, 2278−2281.
(44) Ogo, S.; Makihara, N.; Kaneko, Y.; Watanabe, Y. *Organometallics* **2001**, *20*, 4903−4910.
(45) Maenaka, Y.; Suenobu, T.; Fukuzumi, S. *J. Am. Chem. Soc.* **2012**, *134*, 367−374.
(46) Saker, O.; Mahon, M. F.; Warren, J. E.; Whittlesey, M. K. *Organometallics* **2009**, *28*, 1976−1979.
(47) Suzuki, T.; Morita, K.; Tsuchida, M.; Hiroi, K. *Org. Lett.* **2002**, *4*, 2361−2363.
(48) Kramer, C.; Gedeck, P.; Meuwly, M. *J. Chem. Theory Comput.* **2013**.
(49) Devereux, M.; Meuwly, M. *J. Chem. Inf. Model.* **2010**, *50*, 349−357.
(50) Doman, T. N.; Landis, C. R.; Bosnich, B. *J. Am. Chem. Soc.* **1992**, *114*, 7264−7272.
(51) Pauling, L. *Proc. Natl. Acad. Sci. U.S.A.* **1978**, *75*, 569−572.
(52) Schmid, M.; Nogueira, E. S.; Monnard, F. W.; Ward, T. R.; Meuwly, M. *Chem. Sci.* **2012**, *3*, 690.
(53) Law, M.; Hutson, J. *Comput. Phys. Commun.* **1997**, *102*, 252−268.
(54) Breneman, C. M.; Wiberg, K. B. *J. Comput. Chem.* **1990**, *11*, 361−373.
(55) Singh, U. C.; Kollman, P. A. *J. Comput. Chem.* **1984**, *5*, 129−145.
(56) Besler, B. H.; Merz, K. M.; Kollman, P. A. *J. Comput. Chem.* **1990**, *11*, 431−439.
(57) Rappe, A. K.; Casewit, C. J.; Colwell, K. S.; Goddard, W. A.; Skiff, W. M. *J. Am. Chem. Soc.* **1992**, *114*, 10024−10035.
(58) Halgren, T. a. *J. Am. Chem. Soc.* **1992**, *114*, 7827−7843.
(59) Ryckaert, J.-P.; Ciccotti, G.; Berendsen, H. J. C. *J. Comput. Phys.* **1977**, *23*, 327−341.
(60) Huang, J.; Häussinger, D.; Gellrich, U.; Seiche, W.; Breit, B.; Meuwly, M. *J. Phys. Chem. B* **2012**, *116*, 14406−14415.
(61) Jorgensen, W. L.; Chandrasekhar, J.; Madura, J. D.; Impey, R. W.; Klein, M. L. *J. Chem. Phys.* **1983**, *79*, 926−936.
(62) Andersen, H. C. *J. Chem. Phys.* **1980**, *72*, 2384−2394.
(63) Nosé, S.; Klein, M. *Mol. Phys.* **1983**, *50*, 1055−1076.
(64) Hoover, W. *Phys. Rev. A: At. Mol. Opt. Phys* **1985**, *31*, 1695−1697.
(65) Wolinski, K.; Hinton, J. F.; Pulay, P. *J. Am. Chem. Soc.* **1990**, *112*, 8251−8260.
(66) Zhao, Y.; Truhlar, D. G. *Theor. Chem. Acc.* **2007**, *120*, 215−241.
(67) Yu, W.; He, X.; Vanommeslaeghe, K.; MacKerell, A. D. *J. Comput. Chem.* **2012**, *33*, 2451−2468.